BIOCHEMISTRY
including biophysical chemistry & molecular biology

Article

pubs.acs.org/biochemistry

Interactions of the Acyl Chain with the *Saccharomyces cerevisiae* Acyl Carrier Protein

Daniel R. Perez, Marc Leibundgut, and Gerhard Wider*

Institute of Molecular Biology and Biophysics, ETH Zurich, Otto-Stern-Weg 5, 8093 Zurich, Switzerland

Supporting Information

ABSTRACT: Acyl carrier protein (ACP) domains are critical integral components of multifunctional type I fatty acid synthases (FAS I) and polyketide synthases (PKSs), where they shuttle the growing adducts of the synthesis between the catalytic domains. In contrast to ACP of mammalian FAS I, PKSs, and the dissociated fatty acid synthase type II systems (FAS II) of bacteria, fungal FAS I ACP consists of two subdomains, one comprising the canonical ACP fold observed in all FAS systems and the other representing an extra structural subdomain. While ACPs of dissociated FAS II are able to sequester the reaction intermediates during substrate shuttling, such a transport mechanism has not been observed in ACP domains of multifunctional FAS I and PKS systems. For a better understanding of the interaction between the canonical subdomain of fungal ACP with the growing acyl chain and the role of the structural subdomain, we determined the structure of the isolated *Saccharomyces cerevisiae* acyl carrier protein (ScACP) domain by NMR spectroscopy and investigated the interactions between ScACP and covalently attached substrate acyl chains of varying length by monitoring chemical shift perturbations. The interactions were mapped to the hydrophobic core of the canonical subdomain, while no perturbations were detected in the structural subdomain. A population analysis revealed that only approximately 15% of covalently attached decanoyl chains are sequestered by the ACP core, comparable to the mammalian FAS I and multifunctional PKS systems, which do not sequester their substrates. Finally, denaturation experiments show that both ScACP subdomains unfold cooperatively and that the weak interaction of the acyl chain with the hydrophobic core does not significantly affect the ACP stability.

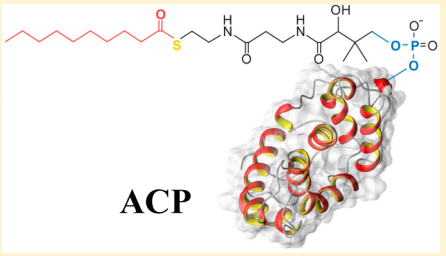

The fatty acid biosynthesis is a metabolic pathway crucial for the survival of prokaryotes and eukaryotes. In most prokaryotes, plants, and parasites, the synthesis resides in enzymes that are dissociated in the cytoplasm, forming the so-called type II fatty acid synthase (FAS II).[1,2] In contrast, most other eukaryotes and *Mycobacteria* harbor type I fatty acid synthases (FAS I), giant multifunctional enzyme complexes into which all catalytic activities necessary for the synthesis of saturated fatty acids are integrated.[3−5] The resulting spatial proximity and high local concentration of the catalytic domains is thought to increase the efficiency of the fatty acid synthesis reaction.[6,7] The global architecture of the type I FAS varies considerably: In yeast, the multifunctional FAS complex is encoded by two different genes, the products of which build up a barrel-shaped heterododecamer containing two reaction chambers, each one harboring three full sets of catalytic sites, thereby performing the simultaneous elongation of six fatty acyl chains,[4,8−10] while in mammals FAS consists of a single polypeptide, which assembles into an X-shaped homodimer.[5] Closely related to mammalian FAS I, polyketide synthases (PKSs) not only share homology on the individual domain level, but also in their overall organization.[11,12] They synthesize polyketides, biologically and pharmaceutically relevant natural products, and the understanding of the mechanisms of delivery of substrates to different catalytic components may provide an opportunity to manipulate and modify the final product of pharmacological active natural substances.[13] Thus, although the structural buildup of the FAS systems largely varies between kingdoms, the underlying chemistry is conserved between all these different fatty acid synthases.

The acyl carrier protein (ACP) is a key component of the fatty acid synthase (FAS) as well as in the biosynthesis of polyketides. ACP acts as an anchor of the growing fatty acid chain, transporting it from the active site of one enzyme to the next.[14,15] The growing acyl chain is held by a thioester linkage to a phosphopantetheine moiety, which is attached via a phosphodiester bond to ACP at a conserved serine residue.[16] In the bacterial type II FAS, ACP consists of a single domain formed by four α helices,[17] which represents the canonical ACP fold. In the structures of spinach FAS II ACP,[18] *Escherichia coli* FAS II ACP (EcACP)[19] and the type II PKS actinorhodin ACP of *Streptomyces coelicolor*,[20] the covalently attached reaction intermediates of the synthesis are engulfed in a hydrophobic cavity in the protein. This suggests that the fatty acid chain delivery to the catalytic domains consists of a switchblade mechanism, in which ACP sequesters the acyl chain to increase the solubility of the reaction intermediate and shields it from unwanted side reactions, then diffuses to the next subunit of FAS and releases the growing chain into the catalytic cleft of

Received: November 25, 2014
Revised: March 13, 2015
Published: March 16, 2015

DOI: 10.1021/bi5014563
Biochemistry 2015, 54, 2205−2213

the enzyme upon interaction. The high ACP concentration found in the *E. coli* cytoplasm (~100 μM) reflects the way in which nature has managed to overcome the problems of an otherwise inefficient mechanism due to large diffusion distances between the individual FAS components.[21] This effect is minimized in type I megasynthases and multifunctional PKSs, where the ACP domain forms an integral part of the biosynthetic machinery, resulting in reduced diffusion distances between the enzymes and very high local concentrations of ACP (>1 mM) and catalytic sites due to compartmentalization. This substrate channeling improves the catalytic efficiency of the FAS even further.[6]

The different overall architectural settings of the PKS, FAS I, and II systems might also result in differences between the mechanisms of transport and delivery of the growing chains by ACP. In animal FAS I, the NMR structure of the rat canonical ACP domain linked to a synthesis intermediate showed no perturbation in the protein upon covalently attachment of the acyl chain, except for the attachment point itself.[22] In this mammalian multidomain FAS complex, the proximity between the catalytic subdomains may allow the transport of a growing acyl chain exposed to the solvent without the need to be engulfed by ACP, as it occurs in type II FAS.[19] NMR studies of the ACP domains from the *Aspergillus* norsolonic acid synthase[23] and the iterative polyketide synthase CalE8 from *Micromonospora*[24] also revealed that in these multifunctional PKSs, the reaction intermediates are not sequestered.

In contrast to the canonical ACP, the ACP domain (ScACP) from *Saccharomyces cerevisiae* FAS I (ScFAS) consists of two subdomains.[9] The canonical subdomain, which is homologous to the ACP from mammals (type I FAS), bacteria, and plants (type II FAS), harbors the attachment point for the growing acyl chain, while the structural domain consists of four additional α helices only found in fungal-type FASs.[9] In the crystal structure of the ScFAS, the ACP domain was observed stalled at the catalytic cleft of the ketoacyl synthase with the phosphopantetheine arm flipped into the active site, and it was suggested that the acyl chain is shuttled and delivered by a switchblade mechanism in analogy to bacteria.[9,19] However, the observation that in mammalian FAS I and PKSs, a switchblade mechanism was not detected,[22−24] and the unclear influence of the additional domain for substrate shuttling and delivery via the canonical part of ScACP lead us to further investigate the role of acyl chain binding on ScACP.

Here we confirm that the structure of the ScACP domain in solution adopts the same fold compared to the stalled ACP in the crystal structure of the entire multifunctional FAS I complex,[9] and that the two subdomains are in a similar conformation relative to each other. In NMR and stability studies at equilibrium, we address how ScACP interacts in solution with growing acyl moieties covalently attached to it, and we discuss the results in the context of the possible mechanism of delivery of the growing acyl chain to the catalytic domains of the FAS complex.

MATERIALS AND METHODS

Protein Expression and Purification. The proteins were expressed in *E. coli* C41 (DE3) transformed by electroporation at 2 kV, 200 Ω, 25 μF using a 50 μL cuvette and a Gene Pulser II from (Biorad, USA) with pET28 containing the ScACP sequence corresponding to the fragment 138−302 of the chain α of ScFAS synthase, and carrying a kanamycin resistance. After selection of a single colony on an agar plate containing 15 μg of kanamycin, the transformed *E. coli* was grown in 2 L of minimal media M9 containing ^{15}N-labeled NH_4Cl and uniformly ^{13}C-labeled glucose. The cultures were grown at 37 °C and 110 rpm, until O.D. 0.7 was reached, and then induced with 1 mM isopropyl β-D-1-thiogalactopyranoside (IPTG) for 6 h before harvesting. The cells were disrupted using a prechilled microfluidizer (Microfluidics Corp, USA) with a working pressure of 80 psi in a lysis buffer (phosphate buffer 50 mM, pH 8.0, 300 mM KCl, imidazole 10 mM, antiproteases cocktail complete EDTA free (Roche), and PMSF 1 mM, DNase I 0.01 mg/mL). The lysate was centrifuged at 4 °C at 35 000 rpm for 90 min in a Beckman Coulter Optima L-90K ultracentrifuge using a Ti45 rotor. The supernatant was batch loaded on 25 mL Ni-NTA agarose (Qiagen), and the slurry was placed in a glass column and mounted in an Äkta FPLC system (Amersham). The resin was washed with 5 CV of washing buffer (phosphate buffer 50 mM, pH 8.0, 300 mM KCl, imidazole 20 mM) at 0.15 mL/min and eluted with a linear gradient 20−150 mM imidazole at 2 mL/min in 14 CV.

Aliquots of each step of the purification were analyzed by 15% acrylamide resolutive and 4% acrylamide stacking SDS-PAGE with a prestained protein molecular weight marker (Fermentas), applying 60 V for the stacking region and 120 V for the resolutive part. The resulting bands were stained with colloidal Coomassie brilliant blue G-250 (Biorad) 0.02% in 2% phosphoric acid, 5% $Al_2(SO_4)_3$, and 10% ethanol,[25] and destained with H_2O. The final sample was analyzed by mass spectrometry (MS) at the Functional Genomic Center Zürich, University of Zürich.

The fractions obtained from Ni-NTA agarose were pooled, and the buffer was exchanged using a HiPrep 26/10 desalting column (Amersham) equilibrated with 20 mM Tris pH 8.0 at 10 mL/min. Afterward, the peaks from the desalting step were pooled and further purified with anion exchange chromatography using an Äkta HPLC equipped with a MonoQ 10/10 (Amersham), equilibrated with 20 mM Tris pH 8.0. The proteins were eluted by a linear gradient 0−300 mM KCl in 14 CV at 1.5 mL/min. The samples were concentrated to 3 mL by centrifugation at 3000*g* in Millipore-Amicon Ultracel-15 centrifugal filter units with regenerated cellulose 10 kDa MWCO. The samples were finally separated by gel filtration loading them into a XK 26/60 column with Superdex200 in an Äkta HPLC and eluting them at 3 mL/min.

Apo- to Holo- and Acyl-holo-ScACP Modification. The modification of ScACP from the apo- to the holo- form was obtained using the reaction with CoA catalyzed by the *S. cerevisiae* phosphopantetheine transferase (ScPPT) domain. An N-terminally His-tagged version of the PPT domain was obtained by cloning residues 1746−1887 of the FAS α chain into a pET28-derived vector. ScPPT was heterologously overexpressed in *E. coli* C41 (DE3) and purified via a Ni-NTA agarose column.[26] The ScACP modification reaction was carried out in a solution with 50 μM ScACP and 0.5 μM ScPPT, 30 mM potassium phosphate at pH 7.5, 5 mM DTT, 10 mM $MgCl_2$, at 28 °C; this reaction mixture was incubated for 90 min. The reaction was stopped by cooling down to 4 °C. The sample was repurified with gel filtration and concentrated by centrifugation as described above.

CoA, hexanoyl-CoA, octanoyl-CoA, and decanoyl-CoA obtained from Sigma were used as substrates for the charging reaction, yielding the acyl-phosphopantetheine derivatives of ScACP. The correct modification was verified by mass spectrometry. Previous to the MS analysis, the samples were

DOI: 10.1021/bi5014563
Biochemistry 2015, 54, 2205−2213

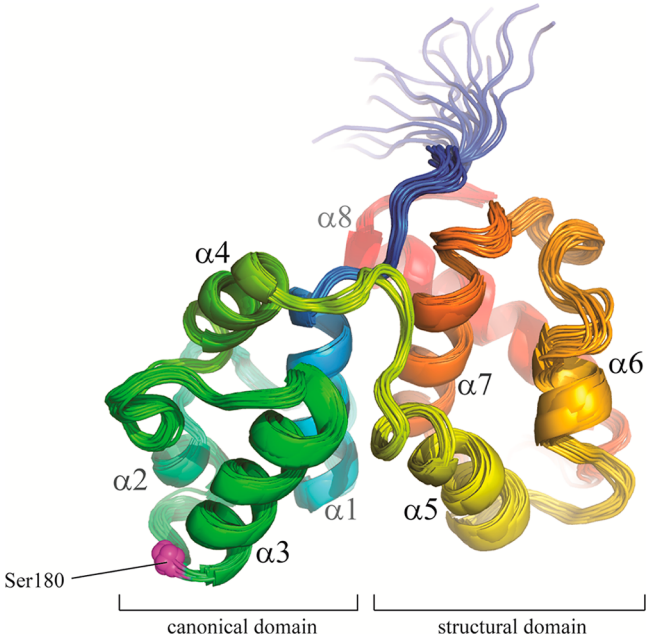

Figure 1. NMR structure of the ScACP fragment (residues 140−302 of the fatty acid synthase α chain) shown as a ribbon diagram of 20 energy minimized conformers, rainbow colored from the N (blue) to the C terminus (red). Helices α1 to α4 of the canonical domain as well as helices α5 to α8 of the structural domain are labeled. The attachment position for the prosthetic group at serine S180 is indicated as a sphere in magenta color.

desalted using C4 ZipTips (Millipore, MA, USA), eluted with 50% acetonitrile/0.2% formic acid (pH 2) and analyzed by electro spray ionization MS (ESI-MS). The m/z data were deconvolved into MS-data using the MaxEnt1 software.

Structure Calculation. Uniformly ^{13}C, ^{15}N-labeled samples of ScACP used for NMR measurements contained 1 mM ScACP in 20 mM phosphate at pH 6.5 in 90% H_2O/10% D_2O. For the structure calculation we recorded one 3D ^{15}N-resolved [^{1}H,^{1}H]-NOE spectrum, and two 3D ^{13}C-resolved [^{1}H,^{1}H]-NOE spectra, where the ^{13}C carrier was placed in the aliphatic and in the aromatic region, respectively. The NOESY spectra were measured with a mixing time of 60 ms, and the NMR data was Fourier transformed and baseline corrected with TOPSPIN 2.1 (Bruker, Karlsruhe, Germany). The spectra were analyzed with the software CARA (www.nmr.ch).

As an input for the structure determination, we used the previously established chemical shift assignment of ScACP that have been deposited in the BioMagResBank (http://www.bmrb.wisc.edu) under the accession number 16085.[26] We performed the standard protocol of seven iterative cycles of NOESY resonances localization and assignment by ATNOS-CANDID and 3D conformer calculation by CYANA.[27−30]

The 20 conformers with the lowest residual CYANA target function values were selected from the cycle 7 to represent the NMR structure and energy minimized using AMBER 12.[31] The structures were analyzed using MOLMOL[32] and PYMOL[33] and are deposited in the Protein Data Bank (PDB) under accession code 2ML8.

Chemical Shift Mapping. [^{15}N,^{1}H]-HSQC spectra of uniformly ^{15}N-labeled samples of apo-, holo-, hexanoyl-, octanoyl-, and decanoyl-ScACP were obtained at 20 °C. The samples were used at concentrations of 1 mM of protein except for decanoyl-ScACP, which was only concentrated to 200 μM;

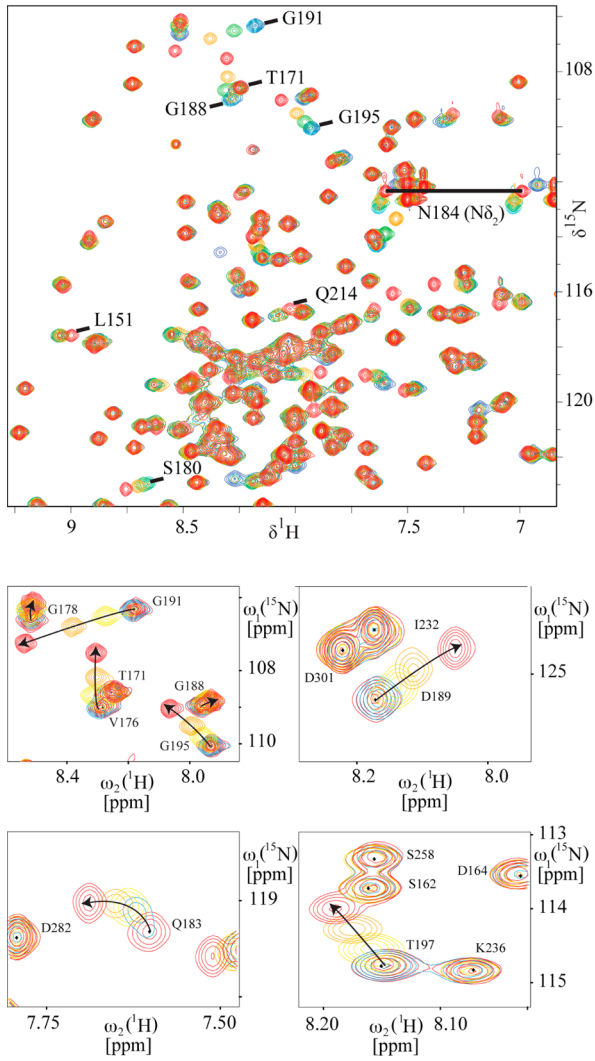

Figure 2. Top: Superimposed [^{1}H,^{15}N] correlation spectra (HSQC) of apo- (dark blue), holo- (cyan), hexanoyl- (green), octanoyl- (orange), and decanoyl- (red) ScACP. The spectra were recorded on a 750 MHz BRUKER spectrometer using uniformly ^{15}N-labeled protein in 20 mM potassium phosphate buffer at pH 6.5. Some of the resonances undergoing the largest chemical shift perturbations upon ScACP modification are indicated by the one letter amino acid code and the sequence number; Nδ_2 refers to the nitrogen side chain NH_2-resonances. Bottom: Expanded regions of the [^{1}H,^{15}N] HSQC spectra: the arrows indicate the direction in which the resonances are shifting upon ScACP modification and acyl chain elongation.

concentrations were measured using PULCON.[34] All samples were measured in 90% H_2O/10% D_2O with 20 mM phosphate at pH 6.5. The spectra were recorded on a Bruker AVIII 750 NMR spectrometer equipped with a ^{1}H,^{13}C,^{15}N triple resonance probe. The HSQC spectra were recorded with $t_{1,max}$ (^{15}N) = 100 ms, $t_{2,max}$ (^{1}H) = 125 ms. The number of scans was 2 for all the samples with the exception of decanoyl-ScACP, for which 32 scans were measured in order to compensate for the lower concentration.

The combined chemical shift differences, $\Delta\delta$, between the differently modified proteins for the H_X/X resonances in ^{1}H and X (^{15}N or ^{13}C) dimensions were obtained using the formula

$$\Delta\delta = [(\Delta\delta(H_X)^2 + (\Delta\delta(X)/n)^2]^{1/2} \quad (1)$$

with n = 5 for X = ^{15}N, and n = 2 for X = ^{13}C.[35]

DOI: 10.1021/bi5014563
Biochemistry 2015, 54, 2205−2213

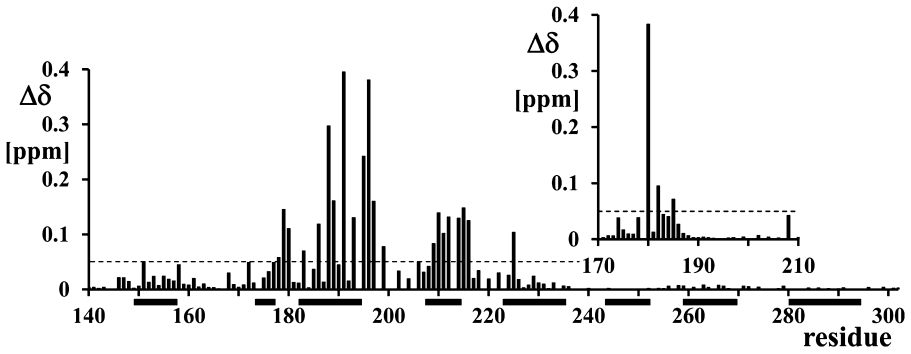

Figure 3. Combined chemical shift perturbations of ^{1}H and ^{15}N nuclei, $\Delta\delta$, between the holo-ScACP and the decanoyl form of ScACP plotted against the residue number; the inset shows the corresponding data for the apo- and holo- forms. The combined chemical shift perturbations of ^{1}H, $\Delta\delta(H_N)$, and ^{15}N, $\Delta\delta(N)$, were calculated with the formula $[(\Delta\delta(H_N)^2 + (\Delta\delta(N)/5)^2]^{1/2}$;[35] an arbitrary threshold of 0.05 ppm was used to define perturbations considered significant. The black horizontal bars indicate the positions of the eight α helices in ScACP.

Filtered 1D ^{1}H NMR Experiments and ^{1}H Assignment of the Decanoyl-phosphopantetheine Group. The ^{1}H NMR spectrum of the acyl chain was measured in a sample containing doubly labeled (^{15}N,^{13}C) ScACP with an unlabeled decanoyl chain attached. In the experiment the magnetization of all protons attached to ^{15}N and ^{13}C is destroyed by a double filter based on INEPT.[36] The assignment of the ^{1}H resonances of the decanoyl-phosphopantetheinyl group attached to the protein was based on the analysis of the following experiments: 2D [^{1}H,^{1}H]-COSY experiment measured with decanoyl-coenzyme A, standard 1D ^{1}H experiment with CoA, the 1D double ^{15}N and ^{13}C filtered data obtained from decanoyl-phosphopantetheine-ScACP (see above). All experiments were measured in 20 mM potassium phosphate buffer at pH 6.5 and 25 °C; the results were compared to a published chemical shift list of palmitoyl-coenzyme A bound to acyl coenzyme A binding protein.[37]

RESULTS

Solution Structure of ScACP and Comparison with Other Structures. We determined the solution structure of the apo- form of ScACP in aqueous solution by NMR spectroscopy to confirm that the crystal[9] and NMR structures adopt the same fold. Figure 1 shows a ribbon representation of the 20 conformers that best satisfied the distance constraints obtained from NOESY experiments. The precision of the bundle of 20 conformers is characterized by an r.m.s.d. of 0.53 Å for the backbone atoms and 0.82 Å for the side chain heavy atoms of residues 140−302 (Table S1, Supporting Information; residue numbering corresponding to the α chain of ScFAS). ScACP in aqueous solution and the X-ray structure of ScACP stalled in the multifunctional FAS I complex[9] adopt the same overall fold with similar orientations of the canonical (residues 140−218) and structural (residues 219−302) subdomains relative to each other (Figure S1A, Supporting Information).

The canonical domain of ScACP, which harbors the attachment site for the growing acyl chain at Ser180, consists of four helices (α1, α2, α3, and α4) in an arrangement closely similar to the X-ray structure, with an r.m.s.d. of 1.16 Å for all superimposed C_α atoms (Table S2, Supporting Information). Compared to the X-ray structure, the NMR structure displays an additional 3_{10} helical turn (residues 163−165) in the segment connecting helices α1 and α2.

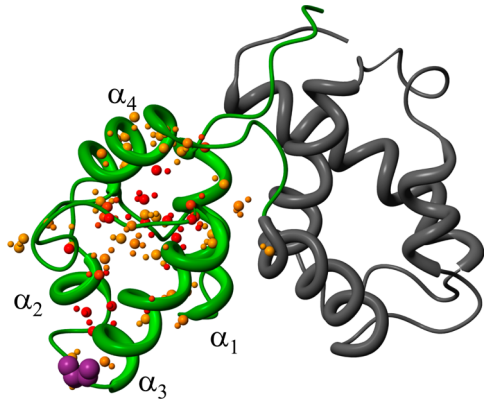

Figure 4. Combined chemical shift perturbations, $\Delta\delta$, of NH-/CH-moieties between [^{1}H,^{15}N]-/[^{1}H,^{13}C]- HSQC spectra of ScACP holo- and decanoyl- forms mapped on the NMR structure. The canonical domain is colored in green and the structural domain is in gray. All atoms with significant $\Delta\delta$ values (see Figures 3 and S4) are shown as small spheres using the following color code: orange: $0.05 \leq \Delta\delta \leq 0.2$ ppm and red: $\Delta\delta > 0.2$; the heavy atoms N and C are shown with larger spheres than hydrogen atoms. Magenta spheres represent Ser 180, where the phosphopantetheine group (not shown) is attached. The orientation of the molecule is the same as in Figure 1; the figure was prepared using the program MOLMOL.[32] For a better visual localization of the individual spheres, a stereoview of this figure and one of the backside of the molecule are shown in Figure S5 in the Supporting Information.

In the structural subdomain, the alignment between the X-ray and the mean NMR structure reveals an r.m.s.d. of 2.40 Å between all C_α atoms, significantly larger than the 1.16 Å observed for the alignment of the helices in the canonical domain. Largest differences are observed at the end of helix α5 and in the loop connecting helices α5 and α6 (residues 232−240), where helix α5 is horizontally displaced between the two structures, and in the loops connecting helices α6 with α7 and α7 with α8, respectively (Figure S1A). This area is in contact with the butterfly-like dimerization module 3 of the central wheel in the stalled FAS complex and may adopt a defined conformation only when bound to an active site (Figure S1B, Supporting Information).

The four helix bundle topology of the canonical ScACP subdomain is similar to other type I and type II ACPs, in spite of low sequence conservation (Table S2, Supporting Information). The low sequence homology is also evident upon inspection of the surface potential of ScACP and comparison

DOI: 10.1021/bi5014563
Biochemistry 2015, 54, 2205−2213

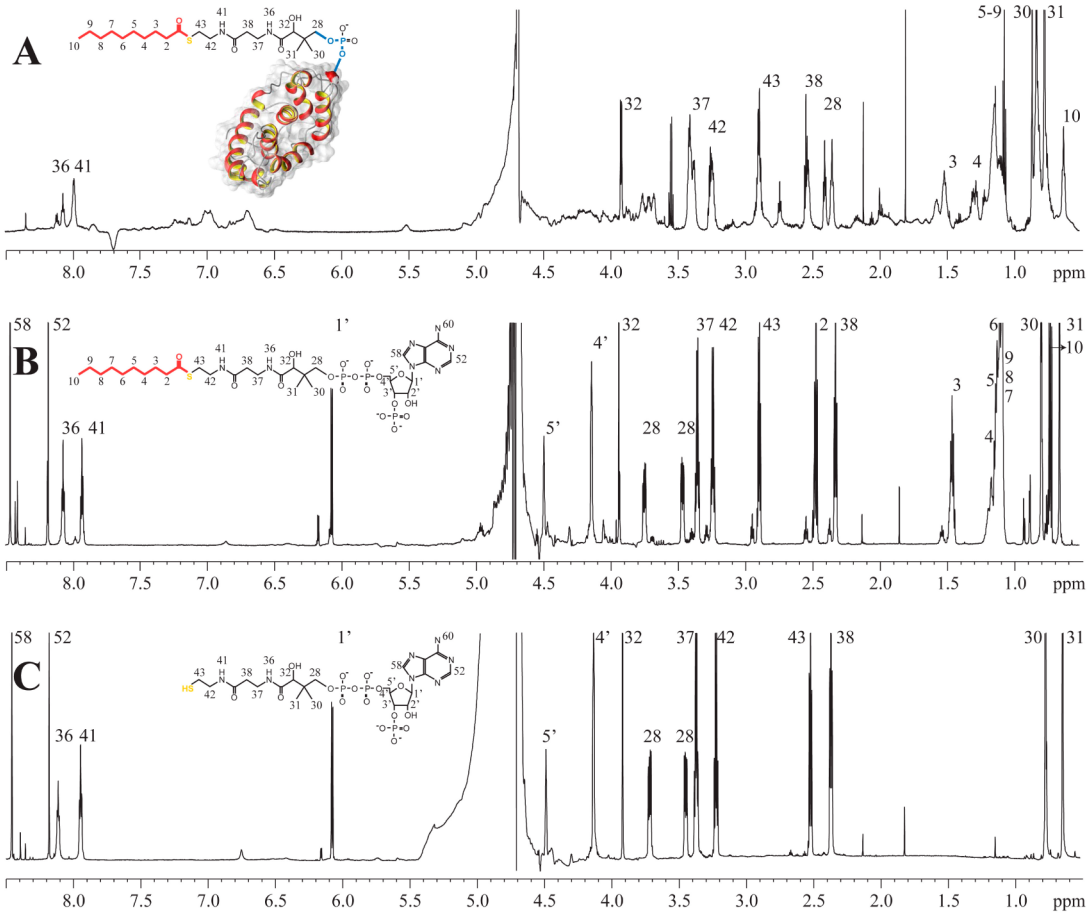

Figure 5. 1D ^{1}H NMR spectra measured at 750 MHz showing assignments of resonances of different compounds in 20 mM phosphate buffer at pH 6.5 in 90%/10% H_2O/D_2O solution, at 25 °C. (A) Unlabeled decanoyl-phosphopantetheine group covalently attached to (^{15}N,^{13}C) uniformly labeled Sc-ACP; signals of ^{1}H attached to ^{15}N or ^{13}C are suppressed (see main text); (B) 1D ^{1}H spectrum of decanoyl-coenzyme A. (C) 1D ^{1}H spectrum of coenzyme A.

with the surface potential of other type-I ACPs, revealing fundamental differences in the canonical subdomain, which may represent an adaptation to specific functions or overall architectural differences between the multienzymes (Figure S2, Supporting Information).

Modification of Apo- into Holo- and Acyl-ScACP. For the modification of apo-ScACP with saturated acyl chains of different length, we used an *in vitro* assay with recombinantly overexpressed and purified *S. cerevisiae* phosphopantetheinyl transferase (ScPPT) and ScACP domains. With this procedure, we obtained the holo- form carrying the prosthetic phosphopantetheine group and three variants carrying acyl chains of three different lengths (hexanoyl-, octanoyl-, and decanoyl-chains). The quality of the modification products was analyzed by MS (Supporting Information, Figure S3).

Chemical Shift Perturbations upon ScACP Modification. The mean structure of the bundle of 20 conformers representing the NMR structure was used to visualize the NMR chemical shift perturbations upon ScACP modification from apo- to different acyl holo-forms. We used [^{1}H,^{15}N] and [^{1}H,^{13}C] NMR correlation spectra (HSQCs) to compare the apo- form of ScACP with the four modified versions: the holo-, hexanoyl-, octanoyl-, and decanoyl- forms of ACP. Figure 2 shows an overlay of the central regions of the [^{1}H,^{15}N]-HSQC spectra for the five forms of ScACP. Combined chemical shift perturbations larger than 0.05 ppm are observed in 22 backbone amide resonances in the decanoyl-form (Figure 3). The chemical shift perturbations between apo- and holo-ACP are limited to the attachment point at Ser180.

The backbone amide resonances experience a gradual displacement in the spectra of the different forms. There is no line broadening that would indicate an intermediate exchange regime on the NMR time scale. The four expansions in Figure 2 show that some resonances shift linearly, e.g., Gly191 and Thr197, indicative of a transition between two main conformations, and others like Gln183 display curved displacements that indicate exchange between more than two conformations. The chemical shift displacements increase according to the length of the attached molecule, a behavior consistent with a higher affinity of the acyl moiety with growing chain length. The end point of the chemical shift deviation may not have been reached because we could not attach an acyl chain with more than 10 carbon atoms due to ScACP aggregation during the modification reaction.

The combined chemical shift perturbations observed between the ScACP holo- and decanoyl-forms, i.e., those perturbations that can be attributed to the interactions with the C10 acyl chain, were quantified using published relations.[35] The perturbations in the backbone amide as well as all backbone and side aliphatic groups are shown in Figures 3 and S4, respectively. Perturbations are observed only for residues of the canonical domain (harboring Ser180) in ScACP, which line the

DOI: 10.1021/bi5014563
Biochemistry 2015, 54, 2205−2213

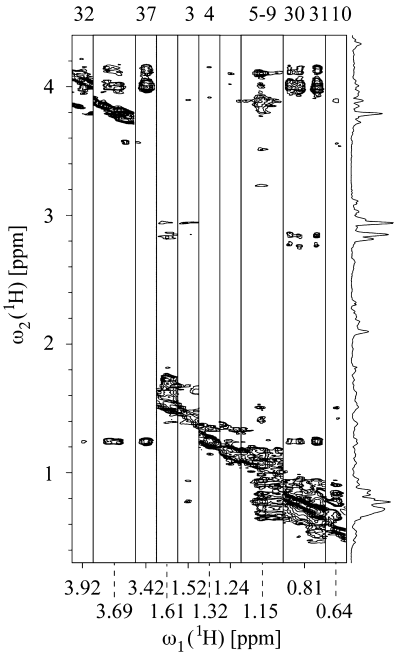

Figure 6. Strips from a 2D ^{13}C ω_1-filtered, ^{13}C ω_2-edited NOESY spectrum (τ_m = 120 ms) of unlabeled decanoyl-phosphopantetheine and ^{15}N,^{13}C labeled ScACP recorded in 90% H_2O/10% D_2O at 25 °C. Acyl chain signals are observed in ω_1, while ^1H chemical shifts of ScACP are recorded in ω_2, respectively.[38] Thus, only intermolecular NOEs between $^1H-^{12}C$ and $^1H-^{13}C$ moieties are seen. Strips are labeled on top with the resonance numbers shown in Figure 5A.

hydrophobic cavity that engulfs the acyl chain in the homologous ACP protein in bacteria.

The chemical shift perturbations were mapped onto a backbone representation of the ScACP NMR structure (Figures 4 and S5). Most nuclei (~70%) with chemical shift perturbations larger than 0.05 ppm are found in the hydrophobic core with an accessible surface area (ASA) < 15%, specifically in the cavity between the helices α2, α3, α4, and the loop connecting α3 and α4, while the remaining chemical shift perturbations stem from solvent exposed atoms with an ASA larger than 15%.

Population of the Acyl Chain Interacting with the Hydrophobic Cavity. The ratio between free and interacting acyl chains allows the characterization of the interaction with the ScACP domain. The ratio was estimated from a line width analysis of resonances of the growing acyl chain. The line width of NMR resonances of a molecule depends on its rotational correlation time, which is much smaller for a chain moving free in solution than for one bound to a globular protein such as ACP. For bound and free forms in fast exchange, the line width is determined by the average between fully bound and free acyl chain weighed by the population in each state. For fully bound acyl chains, the line width is expected to be the same as for the resonances of the protein. A non-interacting acyl chain separated 14 single bonds from the attachment point (see molecule in Figure 5A) would produce practically the same line width as a chain detached from the protein (Figure 5B). This assumption is confirmed by the ^1H resonances 32 and 36 (Figure 5), which have practically the same line width in the 1D ^1H spectrum of decanoyl-coenzyme A (Figure 5B) and the one of decanoyl-phosphopantetheine group covalently attached to Sc-ACP (Figure 5A); other resonances confirm this finding, but are harder to quantify exactly due to overlap. For the population analysis, we determined the ^1H line widths of resonances of the decanoyl-acyl chain in soluble decanoyl-CoA in the absence of ACP (Figure 5B) and of the protein ^1H resonances at full width at half-maximum (fwhm) to be 1.8 and 22.1 Hz, respectively.

The ^1H NMR spectrum of the decanoyl-chain attached to the protein was measured in a sample containing doubly labeled (^{15}N,^{13}C)-ScACP with an unlabeled decanoyl chain attached. The ^1H resonances attached to the protein could thus be suppressed by a heteronuclear filter leaving observable only ^1H resonances of the acyl chain (Figure 5A). The assignments of the ^1H resonances of the acyl chain in the one-dimensional ^1H spectrum were obtained as described in Materials and Methods. The measured ^1H line width for the resonance at 0.63 ppm of the methyl group at the end of the acyl chain (C10) attached to ScACP is 4.2 Hz. Thus, a linear interpolation suggests a bound population of approximately 10−15% under the assumption that the C10 methyl tumbles with the protein; otherwise the population becomes higher. The other resonances of the acyl chain are overlapping, and reliable line widths cannot be obtained. Nevertheless, line width estimations exclude a bound population of larger than approximately 25%. Further, the NH groups 36 and 41 in the linker produce separated resonances. However, the line widths of these resonances are affected by residual exchange with the hydrogens of the water molecules, which may influence the line width in the free and bound form differently. Still, one can deduce an upper limit of the bound form of about 25%. Thus, the rough line width estimations suggest a population of the bound form between 10 and 25%.

NOE Transfer between the Acyl Chain and the Protein. Despite the low population of the acyl chain that interacts with the protein, using a 2D filtered/edited NOESY experiment,[38] we were able to detect interactions between the acyl chain and the protein. In Figure 6, NOE data from the phosphopantetheine-decanoyl chain are shown, which correspond to seven dispersed ^1H resonances and one degenerated peak (comprising methylenes 5−9, Figure 5A). We observed NOEs between ^1H resonances from the acyl chain (ω_1 dimension) and protein ^1H resonances (ω_2 dimension) mainly in the spectral regions 3.8−4.2 ppm and 0.4−1.4 ppm, with some small NOEs for the region between 2.8−3.0 ppm. Because of the crowding of resonances in these spectral regions, the protein resonances could not be individually assigned.

Stability of ScACP upon Modification with Growing Acyl Chains. In order to investigate the influence of the interaction of the acyl chain with the canonical domain on the overall stability of ScACP, we monitored thermal and urea denaturation transitions at equilibrium using circular dichroism (CD) (see Supporting Information). The temperature transition curves suggest that decanoyl-ScACP is less stable than holo-ScACP and apo-ScACP (Figure 7A). However, the thermal unfolding was not reversible, and the influence of aggregates on the measurements could not be quantified. In this situation we also measured chemical denaturation by urea, where no differences were detectable upon acyl chain modification when taking measurement errors into account (Figure 7B−D). While chemical denaturation shows no influence of acyl binding on the overall ACP stability, the irreversible thermal denaturation indicates a reduction in stability with increasing length of the attached acyl chain (Figure 7A). Although we do not exactly understand this discrepancy, one could speculate that the denaturant floats the acyl chain, which is only weakly interacting with the intact

DOI: 10.1021/bi5014563
Biochemistry 2015, 54, 2205−2213

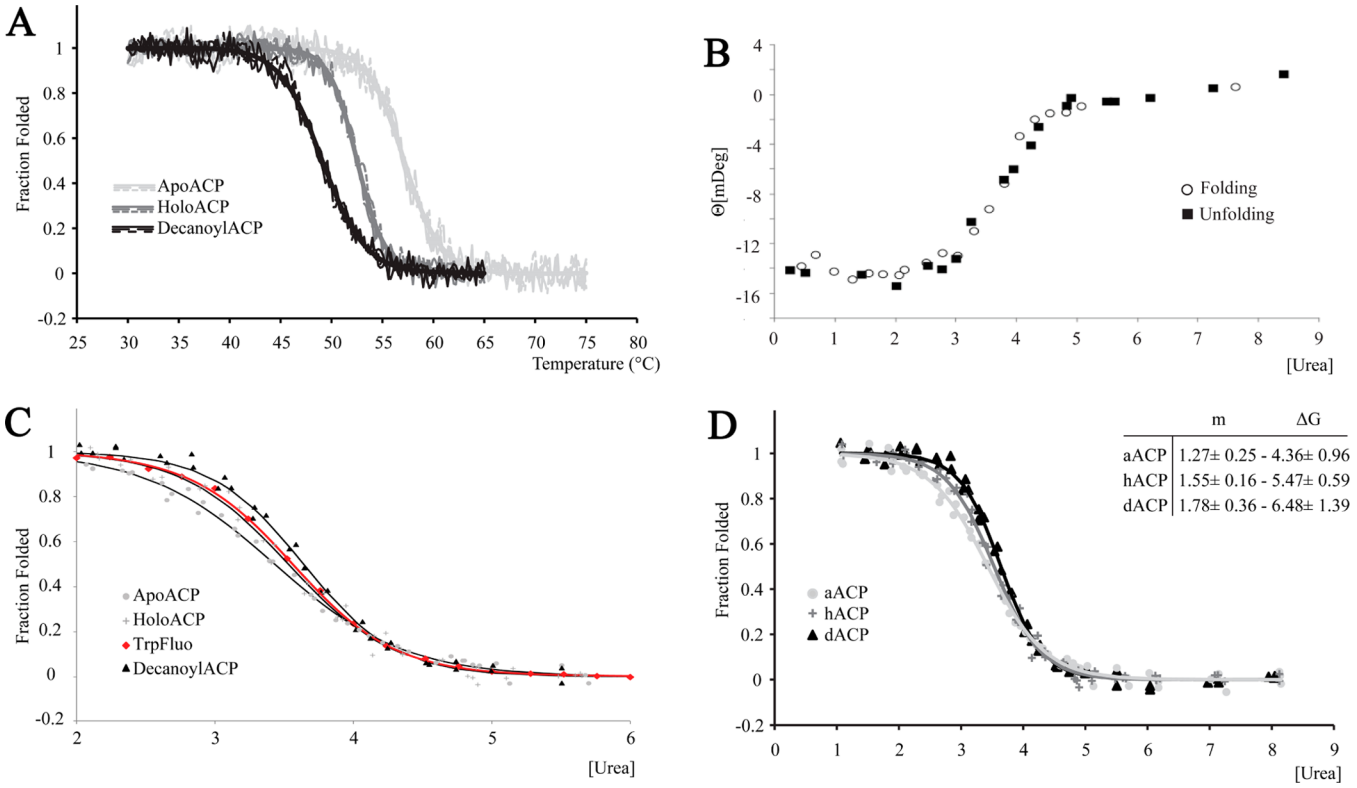

Figure 7. Denaturation of different ScACP forms in 20 mM phosphate buffer at pH 6.5. (A) Thermal denaturation monitored by circular dichroism (CD) spectroscopy at 210 nm using a continuous temperature change at a rate of 0.2 °C/min, and 2 nm bandwidth. The curves represent apo-ScACP (light gray), holo-ScACP (dark gray), and decanoyl-ScACP (black) with denaturation midpoints at 57.1 °C, 52.5 °C, and 49.1 °C, respectively. (B–D) Chemical denaturation of ScACP by urea. (B) Denaturation and refolding curves for 5 μM ScACP monitored by CD; the ellipticity at 220 nm is shown for the chemical unfolding by urea (squares), and refolding by delution (circles). (C) Unfolding of holo-ScACP monitored by tryptophan fluorescence at 520 nm (red curve and symbols); normalized denaturation data obtained by CD at 220 nm (black curves) are shown for apo- (circles), holo- (crosses), decanoyl- (triangle) ScACP. (D) The normalized ellipticity at 220 nm upon addition of urea after 3 h of equilibration of apo- (closed circles), holo- (crosses), and decanoyl-ScACP (triangle); the *m*-values and ΔG for the three forms are indicated in the figure.

protein. Thus, the chemical denaturation of ACP might be independent of the length of the acyl chain. With thermal denaturation, the hydrophobic interactions between the acyl chain and the protein increase with chain length and temperature, leading to reduced stability and aggregation.

DISCUSSION

On the basis of our measurements, yeast ACP interacts only weakly with the covalently attached acyl chain. Assuming a two state on/off model, 10–25% of the acyl chains are bound to the ScACP domain. All the interactions we measured by NMR were in the canonical domain, and most of the affected residues are located in the hydrophobic core between helices α3 and α4, while no significant perturbation was detected in the structural domain of ACP.

The fatty acid synthesis in bacteria is accomplished in the cytoplasm by independent soluble components.[1,2] This FAS II system is rather inefficient and requires 100 μM concentration of soluble ACP, so far the highest described concentration of a single protein in the bacterial cytoplasm.[21] Since the catalytic FAS components are not linked to each other, the bacterial ACP has to diffuse in the cytoplasm from one catalytic site to the next one. Thus, it seems more important to protect the labile thioester bond between the prosthetic group and the acyl chain against hydrolysis than to optimize the availability of the growing fatty acid from the ACP shuttle at the next active site. In *E. coli* for example, the ACP engulfs the growing acyl chain to protect the labile bond,[19] although this could reduce the rate with which the acyl chain can be released.

In multifunctional FAS I systems, the efficiency of the fatty acid biosynthesis is improved by increasing the effective concentration of the components in the reaction and by a simplified gene regulation, which warrants an optimal stoichiometry of the individual catalytic activities and ACP in the reaction. For fungal FAS, a switchblade-like sequestration of the acyl moiety by ACP has been postulated based on analogy to bacteria.[9,18,19] However, our findings demonstrate that ACP sequesters only a minor fraction of the acyl chain, which is in line with the results obtained for mammalian FAS I in rat, where no interaction was detected between the ACP and the acyl chain,[22] and ACPs from multifunctional PKSs.[23] It seems that in FAS I systems, evolution has found another way to further improve the efficiency of the system by selecting mutations in the ACP domains of mammals and fungi in a way that it does not engulf the growing acyl chain, so that it is readily available for interactions with the active sites of the catalytic components.

Stability measurements of the different forms of ScACP by chemical denaturation indicate only marginal differences within the error range of the measurement. The stability studies were made in solution, which resembles the state of the ACP while shuttling the synthesis intermediate between the catalytic sites

DOI: 10.1021/bi5014563
Biochemistry 2015, 54, 2205–2213

inside the reaction chambers of FAS I. The attachment of an acyl chain to ScACP seems not to have a measurable influence on the structural integrity of ScACP.

With respect to the function of the structural domain, we did not observe any perturbation upon the acyl chain attachment, indicating that the structural domain is not involved directly in substrate delivery. Analysis of the crystal structure of ScACP (2UV8)[9] shows that the interface between the canonical and the structural domains comprises 26 residues forming an extensive surface area of approximately 630 A^2. Two buried hydrogen bonds are found between Asp189 Oδ2 and Glu224 Nϵ2 and between Glu193 Oϵ1 and Ser225 H_N, and one buried salt bridge is present between His157 Nϵ2 and Glu272 Oϵ2, all accounting for a calculated stability upon complexation of −10.9 kcal/mol. Our CD (average of both domains) and fluorescence (single tryptophan reports on the structural domain) measurements of the unfolding process indicate that the interface determines the cooperative unfolding, since the two measurements coincide and a two state model applies. The large interface area between the canonical and the structural domain, the fact that they fold cooperatively, and the similar stabilities of holo- and decanoyl-ACP support the idea that the function of this structural domain is a more static one and helps keeping the overall stability of the ScACP domain rather than influencing the binding of the acyl chain. However, considering the surface charge distribution of both the structural and canonical subdomains (Figure S2), the latter being fundamentally different from ACPs of other multifunctional enzymes, it is possible that the extra ScACP subdomain evolved together with the canonical subdomain to optimally interact with the catalytic clefts in the interior of the reaction chamber in the FAS complex (Figure S1B). This is exemplified for the ScACP bound to the ketoacyl synthase (KS) domain in the context of the whole complex, where the ACP binds to the negatively charged central wheel via an extensive patch of complementary charge, involving both the canonical and structural subdomains.[9]

■ ASSOCIATED CONTENT

Supporting Information

Analysis of the ScACP modifications by mass spectroscopy. Description of thermal and chemical denaturation. Figure S1: Comparison of X-ray and NMR ACP structures; Figure S2: Surface potential of ScACP and related enzymes; Figure S3: Mass spectra of apo-, holo- and acyl-ScACPs; Figure S4: Chemical shift perturbations in CH moieties; Figure S5: Chemical shift perturbations mapped onto the ACP structure (stereoviews); Table S1: Input for structure calculation and validation of the energy-minimized NMR structures of ScACP; Table S2: Comparison of ScACP with other published ACP structures; references for Supporting Information. This material is available free of charge via the Internet at http://pubs.acs.org.

■ AUTHOR INFORMATION

Corresponding Author

*Telephone: +41 44 633 3455. Fax: +41 44 633 1484. E-mail: gsw@mol.biol.ethz.ch.

Funding

This research was funded by the Swiss National Science Foundation (SNF) and the ETH Zurich.

Notes

The authors declare no competing financial interest.

■ ACKNOWLEDGMENTS

We acknowledge Dr. Jan Erzberger for the cloning of ScACP and ScPPT, Timm Maier for critically reading the manuscript, Manuela Hess for her contribution in the stability measurements, and Dr. Markus Blatter for support with the NMR structure calculations.

■ ABBREVIATIONS

ACP, acyl carrier protein; ScACP, acyl carrier protein from *Saccharomyces cerevisiae*; FAS I, type I fatty acid synthase; FAS II, type II fatty acid synthase; PKS, polyketide synthases; 2D, two-dimensional; 3D, three-dimensional; HSQC, heteronuclear single quantum coherence; NOE, nuclear Overhauser enhancement; NOESY, 2D NOE spectroscopy; r.m.s.d., root-mean-square deviation

■ REFERENCES

(1) Brindley, D. N., Matsumur, S., and Bloch, K. (1969) Mycobacterium Phlei Fatty Acid Synthetase - a Bacterial Multienzyme Complex. *Nature 224*, 666−669.

(2) White, S. W., Zheng, J., Zhang, Y. M., and Rock, C. O. (2005) The structural biology of type II fatty acid biosynthesis. *Annu. Rev. Biochem.*, 791−831.

(3) Boehringer, D., Ban, N., and Leibundgut, M. (2013) 7.5-angstrom Cryo-EM Structure of the Mycobacterial Fatty Acid Synthase. *J. Mol. Biol. 425*, 841−849.

(4) Jenni, S., Leibundgut, M., Boehringer, D., Frick, C., Mikolasek, B., and Ban, N. (2007) Structure of fungal fatty acid synthase and implications for iterative substrate shuttling. *Science 316*, 254−261.

(5) Maier, T., Leibundgut, M., and Ban, N. (2008) The crystal structure of a mammalian fatty acid synthase. *Science 321*, 1315−1322.

(6) Jenni, S., Leibundgut, M., Maier, T., and Ban, N. (2006) Architecture of a fungal fatty acid synthase at 5 angstrom resolution. *Science 311*, 1263−1267.

(7) Lynen, F. (1980) On the Structure of Fatty Acid Synthetase of Yeast. *Eur. J. Biochem. 112*, 431−442.

(8) Johansson, P., Wiltschi, B., Kumari, P., Kessler, B., Vonrhein, C., Vonck, J., Oesterhelt, D., and Grininger, M. (2008) Inhibition of the fungal fatty acid synthase type I multienzyme complex. *Proc. Natl. Acad. Sci. U.S.A. 105*, 12803−12808.

(9) Leibundgut, M., Jenni, S., Frick, C., and Ban, N. (2007) Structural basis for substrate delivery by acyl carrier protein in the yeast fatty acid synthase. *Science 316*, 288−290.

(10) Lomakin, I. B., Xiong, Y., and Steitz, T. A. (2007) The crystal structure of yeast fatty acid synthase, a cellular machine with eight active sites working together. *Cell 129*, 319−332.

(11) Leibundgut, M., Maier, T., Jenni, S., and Ban, N. (2008) The multienzyme architecture of eukaryotic fatty acid synthases. *Curr. Opin. Struct. Biol. 18*, 714−725.

(12) Maier, T., Leibundgut, M., Boehringer, D., and Ban, N. (2010) Structure and function of eukaryotic fatty acid synthases. *Q. Rev. Biophys. 43*, 373−422.

(13) Cane, D. E., Walsh, C. T., and Khosla, C. (1998) Biochemistry - Harnessing the biosynthetic code: Combinations, permutations, and mutations. *Science 282*, 63−68.

(14) Majerus, P. W., Alberts, A. W., and Vagelos, P. R. (1965) Acyl carrier protein. IV. The Identification of 4′-phosphopantetheine as the prosthetic group of the acyl carrier protein. *Proc. Natl. Acad. Sci. U.S.A. 53*, 410−417.

(15) Pugh, E. L., and Wakil, S. J. (1965) Studies on mechanism of fatty acid synthesis 14. Prosthetic group of acyl carrier protein and mode of its attachment to protein. *J. Biol. Chem. 240*, 4727−4733.

(16) Byers, D. M., and Gong, H. S. (2007) Acyl carrier protein: structure-function relationships in a conserved multifunctional protein family. *Biochem. Cell Biol. 85*, 649−662.

(17) Holak, T. A., Nilges, M., Prestegard, J. H., Gronenborn, A. M., and Clore, G. M. (1988) Three-dimensional structure of acyl carrier

DOI: 10.1021/bi5014563
Biochemistry 2015, 54, 2205−2213

protein in solution determined by nuclear magnetic resonance and the combined use of dynamical simulated annealing and distance geometry. *Eur. J. Biochem. 175*, 9−15.
(18) Zornetzer, G. A., Fox, B. G., and Markley, J. L. (2006) Solution structures of spinach acyl carrier protein with decanoate and stearate. *Biochemistry 45*, 5217−5227.
(19) Roujeinikova, A., Simon, W. J., Gilroy, J., Rice, D. W., Rafferty, J. B., and Slabas, A. R. (2007) Structural studies of fatty acyl-(acyl carrier protein) thioesters reveal a hydrophobic binding cavity that can expand to fit longer substrates. *J. Mol. Biol. 365*, 135−145.
(20) Evans, S. E., Williams, C., Arthur, C. J., Ploskon, E., Wattana-amorn, P., Cox, R. J., Crosby, J., Willis, C. L., Simpson, T. J., and Crump, M. P. (2009) Probing the Interactions of Early Polyketide Intermediates with the Actinorhodin ACP from *S. coelicolor* A3(2). *J. Mol. Biol. 389*, 511−528.
(21) Davis, M. S., and Cronan, J. E. (2001) Inhibition of *Escherichia coli* acetyl coenzyme A carboxylase by acyl-acyl carrier protein. *J. Bacteriol. 183*, 1499−1503.
(22) Ploskon, E., Arthur, C. J., Evans, S. E., Williams, C., Crosby, J., Simpson, T. J., and Crump, M. P. (2008) A mammalian type I fatty acid synthase acyl carrier protein domain does not sequester acyl chains. *J. Biol. Chem. 283*, 518−528.
(23) Wattana-amorn, P., Williams, C., Ploskon, E., Cox, R. J., Simpson, T. J., Crosby, J., and Crump, M. P. (2010) Solution Structure of an Acyl Carrier Protein Domain from a Fungal Type I Polyketide Synthase. *Biochemistry 49*, 2186−2193.
(24) Lim, J., Kong, R., Murugan, E., Ho, C. L., Liang, Z.-X., and Yang, D. (2011) Solution Structures of the Acyl Carrier Protein Domain from the Highly Reducing Type I Iterative Polyketide Synthase CalE8. *PLoS One 6*, No. e20549.
(25) Kang, D. H., Gho, Y. S., Suh, M. K., and Kang, C. H. (2002) Highly sensitive and fast protein detection with coomassie brilliant blue in sodium dodecyl sulfate-polyacrylamide gel electrophoresis. *Bull. Korean Chem. Soc. 23*, 1511−1512.
(26) Perez, D. R., and Wider, G. (2009) H-1, N-15, C-13 resonance assignment of the acyl carrier protein subunit of the Saccharomyces cerevisiae fatty acid synthase. *Biomol. NMR Assign. 3*, 133−136.
(27) Wuthrich, K., Spitzfaden, C., Memmert, K., Widmer, H., and Wider, G. (1991) Protein Secondary Structure Determination by NMR - Application with Recombinant Human Cyclophilin. *FEBS Lett. 285*, 237−247.
(28) Güntert, P. (2004) Automated NMR structure calculation with CYANA. *Methods Mol. Biol. 278*, 353−378.
(29) Herrmann, T., Güntert, P., and Wuthrich, K. (2002) Protein NMR structure determination with automated NOE-identification in the NOESY spectra using the new software ATNOS. *J. Biomol. NMR 24*, 171−189.
(30) Herrmann, T., Güntert, P., and Wuthrich, K. (2002) Protein NMR structure determination with automated NOE assignment using the new software CANDID and the torsion angle dynamics algorithm DYANA. *J. Mol. Biol. 319*, 209−227.
(31) Case, D. A., Cheatham, T. E., Darden, T., Gohlke, H., Luo, R., Merz, K. M., Onufriev, A., Simmerling, C., Wang, B., and Woods, R. J. (2005) The Amber biomolecular simulation programs. *J. Comput. Chem. 26*, 1668−1688.
(32) Koradi, R., Billeter, M., and Wuthrich, K. (1996) MOLMOL: A program for display and analysis of macromolecular structures. *J. Mol. Graphics 14*, 51−55.
(33) Schrödinger, L. (2010) *The PyMOL Molecular Graphics System*, Version 1.3r1.
(34) Wider, G., and Dreier, L. (2006) Measuring protein concentrations by NMR spectroscopy. *J. Am. Chem. Soc. 128*, 2571−2576.
(35) Schumann, F. H., Riepl, H., Maurer, T., Gronwald, W., Neidig, K. P., and Kalbitzer, H. R. (2007) Combined chemical shift changes and amino acid specific chemical shift mapping of protein-protein interactions. *J. Biomol. NMR 39*, 275−289.
(36) Morris, G. A., and Freeman, R. (1979) Enhancement of Nuclear Magnetic Resonance Signals by Polarization Transfer. *J. Am. Chem. Soc. 101*, 760−762.
(37) Kragelund, B. B., Andersen, K. V., Madsen, J. C., Knudsen, J., and Poulsen, F. M. (1993) Three-dimensional structure of the complex between acyl-coenzyme A binding protein and palmitoyl-coenzyme A. *J. Mol. Biol. 230*, 1260−1277.
(38) Zwahlen, C., Legault, P., Vincent, S. J. F., Greenblatt, J., Konrat, R., and Kay, L. E. (1997) Methods for measurement of intermolecular NOEs by multinuclear NMR spectroscopy: Application to a bacteriophage lambda N-peptide/boxB RNA complex. *J. Am. Chem. Soc. 119*, 6711−6721.

DOI: 10.1021/bi5014563
Biochemistry 2015, 54, 2205−2213